Extension of a Two-Step Calibration Methodology to Include Nonorthogonal Sensor Axes

C. C. FOSTER
G. H. ELKAIM
UC Santa Cruz

We present an extension of the nonlinear two-step estimation algorithm originally developed for the calibration of solid-state strapdown magnetometers. We expand the algorithm to include nonorthogonality within a sensor set for both two- and three-axis sensors. Nonorthogonality can result from manufacturing issues, installation geometry, and in the case of magnetometers, from soft iron bias errors. Simulation studies for both two- and three-axis sensors show convergence of the improved algorithm to the true values, even in the presence of realistic measurement noise. Finally the algorithm is experimentally validated on a low-cost solid-state three-axis magnetometer set, which shows definite improvement postcalibration. We note that the algorithm is general and can be applied to any two- or three-axis sensor set (such as accelerometers) with an error model consisting of scale, offset, and nonorthogonality errors.

Manuscript received August 26, 2006; revised December 29, 2006; released for publication July 20, 2007.

IEEE Log No. T-AES/44/3/929754.

Refereeing of this contribution was handled by G. A. Lachapelle.

Authors' address: Dept. of Computer Engineering, UC Santa Cruz, 1156 High St., SOE 3, Santa Cruz, CA 95064, E-mail: (elkaim@soe.ucsc.edu).

I. INTRODUCTION

With the increase in autonomous systems has come an increase in the need for location awareness using sensors that are compact and have low power requirements. Heading based on magnetic north is an approach that has been borrowed from the aviation industry, partly due to the very high cost of north-seeking gyroscopes. Magnetometers, sensors that detect magnetic fields, are often used to determine magnetic north [1]. Due to the significant progress in magnetometery, accurate and reliable heading information can be achieved by employing a small, low-cost, and highly reliable magnetometer. To achieve equal accuracy in heading determination using gyro-compassing would necessitate an expensive, large, and near-navigation grade gyro. In the case where size, cost, or power constraints rule in micro-electro-mechanical (MEM) type gyros, then magnetic heading becomes the only choice.

Anisotropic magnetoresistive (AMR) sensors are compact, low power devices that are capable of measuring magnetic fields. A Wheatstone bridge of permalloy produces a differential output proportional to the direction and magnitude of magnetic fields on the sensitive axis of the bridge, see Fig. 1. Permalloy is a nickel-iron alloy with an electrical resistance that changes based on its orientation to a magnetic field. Multiple bridges can be combined in a single sensor set allowing for two and three axes of sensitivity.

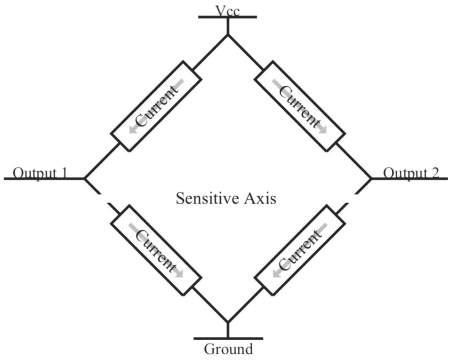

Fig. 1. Four permalloy elements in Wheatstone bridge configuration.

The minimum required to generate a crude heading is magnetic sensitivity in the vehicle body x and y directions. That is, we use the standard aircraft coordinate body frame with the positive x-axis forward out the nose, the positive y-axis out the right wing, and z-axis positive down. For the navigation frame, we use the North-East-Down (NED) coordinate frame such that North is $+x$. Assuming that the vehicle is level, the heading ψ, or angle between a vehicle's positive x-axis and magnetic north, is given by

$$\psi = -\arctan\left(\frac{B_y^b}{B_x^b}\right) \tag{1}$$

where B_x^b is the x-direction component of the Earth's magnetic field in the body fixed reference frame, and B_y^b is the y-direction component. The symbol B is the Earth's magnetic field, and a b superscript refers to body fixed reference frame quantity. An n superscript refers to a navigation fixed reference frame quantity. The subscripts x, y, and z represent the axis of measurement.

Using the raw sensor readings in (1) results in only crude headings as it does not take into account any of the various sources of error in a magnetic field measurement, nor any pitch or roll deviations from a level plane. An accurate heading can be found by developing a mathematical model of the sensor readings that include the sources of error, performing a calibration routine to determine the error coefficients, and finally, processing the raw data to remove the error corruption.

This paper expands upon an algorithm for performing magnetometer and accelerometer calibration originally discussed in [2] and [3]. The procedure detailed here will allow sources of error to be removed from magnetic sensor readings in real time, allowing for accurate heading calculations. We note that the algorithm is general and can be applied to any two- or three-axis sensor set with an error model consisting of scale, offset, and nonorthogonality errors. We note that this algorithm is developed for calibration of three axis magnetometers in a magnetically "clean" environment. That is, the algorithm requires knowledge of the magnitude of the total magnetic field around the vehicle, either this is modeled from the Earth's magnetic field, or an independent, accurate measure of the field is required. Future work will use this same algorithm to calibrate the magnetometers in-situ, using entire vehicle motion, rather than just that of the sensors.

Section II details the errors specific to magnetometer readings. Section III discusses prior art, including the original nonlinear two-step algorithm. Section IV discusses the expanded two-step nonlinear algorithm showing both the two- and three-dimensional cases. Section V shows simulations of both the two- and three-dimensional cases, followed by experimental results of a three-axis sensor set in Section VI. Finally the conclusion of this paper is in Section VII.

II. MAGNETOMETER ERRORS

Any magnetic sensor used to detect the Earth's magnetic field can be influenced by several different sources of error, all combining to corrupt the output. These error sources can be counteracted, but first mathematical modeling and estimation is required. The magnetometer output is typically corrupted due to five error sources, namely: scale factor errors C_{sf}, misalignment errors C_m, null shift errors $\overrightarrow{C_{zb}}$, and finally, hard iron and soft iron errors $\delta\overrightarrow{B^b}$ and C_{si}, respectively. At the physical level, these error sources can be broken into two categories, those caused by the sensors and those inherent in the measuring of magnetic fields. Scale factor errors and null shift errors are a trait of each individual sensing element, and physical misalignment errors are caused by manufacturing tolerances in the construction of sensor sets. Hard iron and soft iron errors on the other hand are side effects of measuring a magnetic field (caused, respectively, by permanent magnetization of ferrous metals induced usually by stress during manufacture, and variable magnetic permeability which causes induced magnetic fields to appear). Despite different physical causes, both error categories appear in the same form mathematically.

The null shift of a sensor, also known as a sensor's dc offset or zero bias, is a constant offset that shifts the output of each sensor. Zero biases are most evident when a sensor is exposed to no magnetic field on the sensitive axis, however the sensor outputs a non-zero value. C_{zb} is a $n \times 1$ vector where n is either 2 or 3 for the two- and three-dimensional cases, respectively, that represents this zero bias error shifting the final output of the each sensor by a constant amount.

The scale error of a sensor is a side effect of varying sensitives between sensors. The sensitivity of a sensor serves to scale the output, and as no two sensors will have the exact same sensitivity it must be determined for each axis independently (note that even sensors in the same integrated circuit (IC) package will often have very different scale factors and null shifts). C_{sf} is an $n \times 1$ vector (where, again, n is either 2 or 3) that accounts for the sensitivities of the individual sensors by scaling the outputs.

The misalignment error of a sensor set comes from a nonorthogonality between individual sensors in the set. When the sensors in a set are aligned properly, a field aligned with only one axis is observed by only one sensor. However, if there is a misalignment, multiple sensors will observe a field that is on only one axis. C_m is an $n \times n$ matrix that accounts for sensor misalignment through scaling the sensor outputs.

The hard iron errors are constant, unwanted magnetic fields observed by a magnetometer. Up to this point we have been careful to define $\overrightarrow{B^b}$ as the Earth's magnetic field, however a magnetometer will pick up any magnetic field, including those not belonging to the Earth. Because hard iron errors must be constant fields, their source must be attached to the same body frame as the magnetometer, otherwise the fields would vary depending on the vehicle's position. $\delta\overrightarrow{B^b}$ is an $n \times 1$ vector that represents the sum of all permanent magnetic fields and shifts

the sensor outputs by a constant amount. Note that mathematically, hard iron errors and null shift errors are indistinguishable.

Unlike hard irons where the field emitted is constant, soft irons are materials that emit their own field in response to exposure to an external field. For the purpose of this paper we will assume that the responses of soft iron materials are linear and without hysteresis such that a square matrix is sufficient. Like with hard iron errors, we only take into account sources that are fixed to the same body frame as the magnetometer. C_{si} is an $n \times n$ matrix that represents the sum of soft iron errors that are fixed to the body frame that serve to scale the sensor outputs.

Combining all five of these error sources into a single mathematical model, the measured magnetic field $\widehat{\overrightarrow{B^b}}$, as a function of the Earth's magnetic field, is

$$\widehat{\overrightarrow{B^b}} = C_m C_{sf} C_{si}(\overrightarrow{B^b} + \delta\overrightarrow{B^b}) + C_{zb}. \tag{2}$$

Note that in this paper we use the $\hat{}$ for measured quantities, not the usual estimated quantities (for estimated quantities, we use the subscript est).

It should be noted that there are additional sources of error that are not included in this model, specifically sources not attached to the vehicle. We have taken into account permanent magnetic fields whose influence on the magnetic sensors do not vary over time, as well as soft iron sources that are fixed to the body frame. We have not taken into account any field with a source not fixed to the body frame, or any fluctuating magnetic fields. Although these error sources are present, they are not included in this model as they would make it too complicated to process.

III. PRIOR ART

Before the original nonlinear two-step calibration algorithm, magnetic sensor sets were typically calibrated through a process called "swinging" [4]. This fairly cumbersome process required putting the sensor set in several known orientations corresponding to specific headings, comparing the output of the sensor set with a reference baseline, and calculating the resulting heading error. Several drawbacks to this approach have been discussed, including the manual process of precisely aligning the sensor set with the predefined orientations, the requirement of a more accurate sensor to provide the reference baseline, and the fact that this routine calibrates the sensor set to the Earth's local magnetic field, requiring recalibration if the sensor set was to travel any significant distance, or very careful factory calibration must be included. Note that in practice, the true orientation of the sensor or vehicle need only be accurate to $\pm 5^\circ$ as long as the arc swung can be measured accurately either by optical or on-board inertial navigation system (INS) sensors.

The nonlinear two-step algorithm developed in [5] avoided many of these drawbacks by solving for the error factors directly in the magnetic domain rather than calibrating the sensor set in the heading domain. The first key to the algorithm is noticing that if one was to plot the output values of an error free or perfect sensor set that was rotated through various angles, those points would fall on top of a circle for the two-dimensional case, or on top of the surface of a sphere for the three-dimensional case (that is: in the 2-D case if we rotated the perfect sensor 360 deg and plotted the points, we would see a perfect circle, centered at [0,0]). The second key is to realize that the various errors in (2) serve only to warp the circle or sphere into a distorted ellipse or, in the three-dimensional case, a distorted ellipsoid.

The nonlinear two-step algorithm in [3] has several advantages over magnetometer swinging. The first is that it applies to any two- or three-axis sensor, not just a magnetometer. Moreover, the method requires no external information other than the data recorded from rotating the sensor and the total magnitude of the vector quantity being measured (that is, no precisely measured angles are required at all). The method is the same as presented in this work, except that the nonorthogonality terms (ρ, ϕ, and λ) are all zero. Again, the measurements taken during sensor/vehicle rotation are stacked, and a least-squares estimate is made for algebraic combinations of the parameters of interest. Then the actual parameter estimates are extracted using algebraic manipulation. For a full treatment of the method, including simulated and experimental results, see [6], [3].

Using these key points, a relationship can be derived between the values that are generated by the rotation of the sensor set and (2). Because this relationship is not linear with respect to the various error sources, a two-step process was developed with the first step solving a linear relationship between the measured values and intermediate variables, and the second step solving an algebraic relationship between these intermediate variables and the error sources. This is an alternative to [7]. Once the error parameters were calculated, these errors could be removed from measurements in real time and an accurate measurement of the Earth's field generated. Heading could be then determined by comparing this corrected measurement to the known magnetic field either as a stright magnetic azimuth calculation, or as one of the two vector measurements required for a Wahba's problem-type full attitude solution. For a quaternion implementation of the Wahba's problem-type attitude solution that uses a three-axis magnetometer and three-axis accelerometer, see [6].

IV. CALIBRATION ALGORITHM DEVELOPMENT

We made three modifications to the original error model, and the resulting changes to the calibration algorithm are presented here. The first two changes are the removal of assumptions made about the sensor misalignment and soft iron errors. The original paper assumed that care would be taken in the assembly of a sensor set such that any sensor misalignment would be negligible. Furthermore, in addition to assuming that soft iron errors could be represented linearly with no hysteresis, the original paper assumed that any soft iron material could be identified and would be positioned far enough from the magnetometer set such that it would have no effect. With the removal of these assumptions, the soft iron error and misalignment error factors will remain in our sensor model.

The final modification to the original error model is the addition of the null offset error. Although the original paper did not account for the null offset error on each sensor, the algorithm produces correct results because the zero bias was simply interpreted as an additional hard iron error. With that said, the zero bias error has been added to (2) in an attempt to be complete, knowing that further calibration beyond that of our algorithm would be required if one cared to separate the hard iron errors from the zero bias errors.

A. Two-Dimensional Case

As stated earlier, the first key to this algorithm is to realize that a plot of the output of an ideal x-y magnetometer leveled and rotated about the z-axis is a circle with a radius equal to the magnitude of the magnetic field to which it was exposed. The second key is to realize that with the addition of the error sources expressed in (2), the circle is altered until it becomes a distorted ellipse. Mathematically, this can be shown as follows.

For a level, error-free x-y magnetometer set, the square of the magnitude of the horizontal component of the Earth's magnetic field is equal to the sum of the square of the x and y components, or the equation of a circle centered at the origin with a radius of B_H:

$$B_H^2 = B_x^{b^2} + B_y^{b^2}. \tag{3}$$

Next the offset and scale factors are added to the equation. Both hard iron and zero bias errors combine to offset the output of the magnetometer set by a constant amount. Because we have no way of mathematically separating these two errors, we will define x_o and y_o as the total offsets in the x and y directions (note that these offsets can be separated physically by using magnetic shielding for a "factory" calibration). sf_x and sf_y are used to represent the x and y components of the scale factor error. Adding these errors to our equations gives

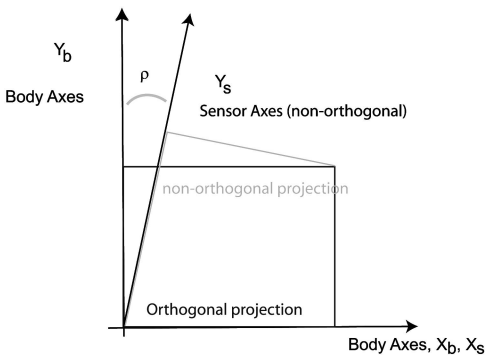

Fig. 2. Sensor axes diagram for nonorthogonality. Note that x-sensor lines up with x-true axis, but that y-sensor is off by angle ρ, which causes y-sensor to respond to both y-component of field and x-component as well.

$$\hat{B}_x^b = sf_x B_x^b + x_o \tag{4}$$

$$\hat{B}_y^b = sf_y B_y^b + y_o. \tag{5}$$

Solving for B_x^b and B_y^b then substituting them into (3) shows the equation of an ellipse shifted off the origin, or:

$$B_H^2 = \left(\frac{\hat{B}_x^b - x_o}{sf_x}\right)^2 + \left(\frac{\hat{B}_y^b - y_o}{sf_y}\right)^2. \tag{6}$$

The final errors come from the two sources previously unexplored, the misalignment errors and soft iron errors. To handle the misalignment error, we assume that the x-sensor is perfectly aligned with the x-axis and we define the misalignment as being between y-sensor and the y-axis. For soft iron errors, they can split into a combination of a scale error and a misalignment error.

Just as with the offset errors, this algorithm will not be able to mathematically separate the total scale errors between scale and soft iron, nor will it be able to mathematically separate the total misalignment error between physical misalignment and soft iron (again, these can be physically determined using other methods to the accuracy required for a "factory" calibration). Therefore a is defined as the total scale error on the x-sensor, b is the total scale error on the y-sensor, and maintaining that the x-sensor as being perfectly aligned with the x-axis, ρ is the total angular misalignment between the y-sensor and the y-axis (see Fig. 2). Note that as can be seen from Fig. 2, the y-sensor senses both the y-axis as well as a part of the x-axis before being scaled. Including these errors into our previous equations gives

$$\hat{B}_x^b = aB_x^b + x_o \tag{7}$$

$$\hat{B}_y^b = b[B_y^b \cos(\rho) + B_x^b \sin(\rho)] + y_o. \tag{8}$$

The result of solving for B_x^b in (7), plugging that into (8) to solve for B_y^b, then plugging both into (3) can be

written in the form of a shifted, distorted ellipse as

$$A\hat{B}_x^{b^2} + B\hat{B}_x^b\hat{B}_y^b + C\hat{B}_y^{b^2} + D\hat{B}_x^b + E\hat{B}_y^b + F = 0 \quad (9)$$

where A, B, C, D, E, and F are functions of a, b, x_o, y_o, and ρ. Equation (9) is not linear in terms of a, b, x_o, y_o, and ρ but is linear in terms of the intermediate variables A, B, C, D, E, and F.

Best estimates for A–F in a least-squares sense can be found by restructuring (9), putting it in matrix form and performing a batch least-squares best fit. Equation (9) can be rewritten as

$$1 = \begin{bmatrix} \dfrac{\hat{B}_x^{b^2}}{\hat{B}_y^{b^2}} & \dfrac{\hat{B}_x^b\hat{B}_y^b}{\hat{B}_y^{b^2}} & \dfrac{\hat{B}_x^b}{\hat{B}_y^{b^2}} & \dfrac{\hat{B}_y^b}{\hat{B}_y^{b^2}} & \dfrac{1}{\hat{B}_y^{b^2}} \end{bmatrix} \begin{bmatrix} -\dfrac{A}{C} \\ -\dfrac{B}{C} \\ -\dfrac{D}{C} \\ -\dfrac{E}{C} \\ -\dfrac{F}{C} \end{bmatrix}. \quad (10)$$

Because A–F are constant for all k measurements, all the data points can be combined into a large matrix equation such that

$$\mathbb{X} \times \mathbb{P} = \mathbb{W} \quad (11)$$

where

$$\mathbb{P} = \begin{bmatrix} -\dfrac{A}{C} \\ -\dfrac{B}{C} \\ -\dfrac{D}{C} \\ -\dfrac{E}{C} \\ -\dfrac{F}{C} \end{bmatrix}^{\mathrm{T}} \quad (12)$$

$$\mathbb{W} = \begin{bmatrix} 1 \\ 1 \\ \cdot \\ \cdot \\ 1 \end{bmatrix} \quad (13)$$

and

$$\mathbb{X} = \begin{bmatrix} \dfrac{\hat{B}_{x_1}^{b^2}}{\hat{B}_{y_1}^{b^2}} & \dfrac{\hat{B}_{x_1}^b\hat{B}_{y_1}^b}{\hat{B}_{y_1}^{b^2}} & \dfrac{\hat{B}_{x_1}^b}{\hat{B}_{y_1}^{b^2}} & \dfrac{\hat{B}_{y_1}^b}{\hat{B}_{y_1}^{b^2}} & \dfrac{1}{\hat{B}_{y_1}^{b^2}} \\ \dfrac{\hat{B}_{x_2}^{b^2}}{\hat{B}_{y_2}^{b^2}} & \dfrac{\hat{B}_{x_2}^b\hat{B}_{y_2}^b}{\hat{B}_{y_2}^{b^2}} & \dfrac{\hat{B}_{x_2}^b}{\hat{B}_{y_2}^{b^2}} & \dfrac{\hat{B}_{y_2}^b}{\hat{B}_{y_2}^{b^2}} & \dfrac{1}{\hat{B}_{y_2}^{b^2}} \\ \cdot & \cdot & \cdot & \cdot & \cdot \\ \cdot & \cdot & \cdot & \cdot & \cdot \\ \dfrac{\hat{B}_{x_k}^{b^2}}{\hat{B}_{y_k}^{b^2}} & \dfrac{\hat{B}_{x_k}^b\hat{B}_{y_k}^b}{\hat{B}_{y_k}^{b^2}} & \dfrac{\hat{B}_{x_k}^b}{\hat{B}_{y_k}^{b^2}} & \dfrac{\hat{B}_{y_k}^b}{\hat{B}_{y_k}^{b^2}} & \dfrac{1}{\hat{B}_{y_k}^{b^2}} \end{bmatrix}. \quad (14)$$

Finally $\mathbb{P}_{\mathrm{est}}$, a least-squares best fit estimate for $\mathbb{P}$, can be calculated as

$$\mathbb{P}_{\mathrm{est}} = (\mathbb{X}^{\mathrm{T}}\mathbb{X})^{-1}\mathbb{X}. \quad (15)$$

Now that estimates for A–F have been found, and assuming B_H is known, solutions for a, b, x_o, y_o, and ρ can be solved algebraically.

B. Three-Dimensional Case

The restriction that the two-dimensional sensor set must remain level while being rotated can be removed through the addition of a z-sensor. Equation 3, no longer just for the horizontal component, but rather the total of the Earth's magnetic field, becomes

$$B^2 = B_x^{b^2} + B_y^{b^2} + B_z^{b^2}. \quad (16)$$

Defining c as the total of all scale factors on the z-sensor, z_o as the total of all offsets on the z-sensor, ϕ as the misalignment angle between the z-sensor from the x-z plane, and λ as the misalignment angle between the z-sensor from the y-z plane, the equation for the magnetic field on the z-sensor is

$$\hat{B}_z^b = c[B_z^b\cos(\phi)\cos(\lambda) + B_x^b\sin(\phi)\cos(\lambda) + B_y^b\sin(\lambda)] + z_o. \quad (17)$$

Solving for B_z^b, (16) can be written in the form of a distorted ellipsoid as:

$$A\hat{B}_x^{b^2} + B\hat{B}_x^b\hat{B}_y^b + C\hat{B}_x^b\hat{B}_z^b + D\hat{B}_y^{b^2} + E\hat{B}_y^b\hat{B}_z^b + F\hat{B}_z^{b^2}F + G\hat{B}_x^b + H\hat{B}_y^b + I\hat{B}_z^b + J = 0 \quad (18)$$

where A, B, C, D, E, F, G, H, I, and J are, again, functions of a, b, c, x_o, y_o, z_o, ρ, ϕ, and λ.

Using the same process as for the two-dimensional case, (18) can be put into matrix form, multiple readings gathered, a batch least-squares estimation for A–J produced, then estimations for the individual calibration parameters solved algebraically. Note that the linearization in this case is along the parameters A-J, and not along the desired parameters $a - \lambda$. In this case, while A-J will be optimal in a least-squares sense, the true parameters a-λ may not necessarily be so. Further work involving geometric projection and numerical solution to the full nonlinear problem has shown that this method produces, in fact, very good estimates. However, formal analysis is for future work. Furthermore, while a posteriori estimates of the covariance is available for A-J, these are not easily transferable through the algebraic manipulations required to extract the parameters of interest.

V. SIMULATIONS

Simulations of this calibration procedure were performed in Matlab for both the two-dimensional and three-dimensional cases.

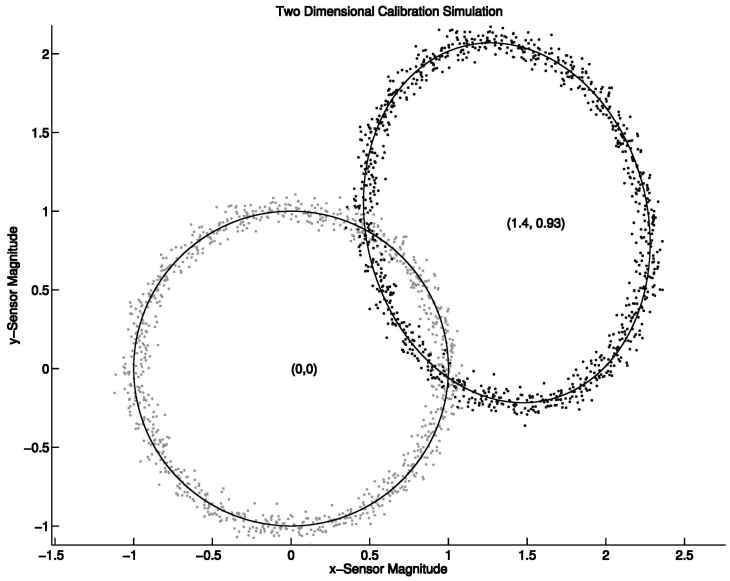

Fig. 3. Two-dimensional simulation of calibration procedure. Uncalibrated data on perimeter of rotated ellipse (upper right) and corrected data on perimeter of circle with radius equal to field strength (lower left), both with center points labeled. Note that units here are in "Earth magnetic field equivalents," and that original offsets in simulation are [1.4,0.98], which are recovered by the algorithm, along with scale factors and nonorthogonality. That is, a perfect sensor would show a circle of radius 1.

A. Two-Dimensional Case

1000 data points are generated in such a way that they simulate a single level rotation of an x-y magnetometer set about the z-axis in a constant field with a magnitude of one. Scale, offset, and misalignment factors are added to simulate the combination all of the error sources discussed in this paper. Random noise up to 5% of the total field strength is added to each reading to account for sensor broadband noise.

Calibration parameters are estimated in Matlab with the procedure presented in this paper then used to reverse the various error sources. Both the raw, corrupted data, and the regenerated data are displayed in Fig. 3. An ellipse based on the estimated error parameters and a circle with a radius of one are also shown to evaluate the accuracy of the fit.

B. Three-Dimensional Case

In the three-dimensional simulation, 5000 data points are generated in such a way that they simulate the sensor set being exposed to a constant field with a magnitude of one while completing five horizontal rotations and half a vertical rotation. DC offsets, scale errors, and misalignments are applied to the data followed by the addition of random noise up to 5% of the magnetic field strength.

Calibration parameters are then estimated with the procedure detailed above and used to remove the errors from the raw data. Fig. 4 shows both the original corrupt data and the final calibrated data along with the estimation ellipsoid and a sphere with a of radius one.

VI. EXPERIMENTAL RESULTS

Only the three-axis case was validated experimentally, and note further that only the "sensor" was rotated, not the entire vehicle. A three-axis magnetometer set was created by combining a two-axis HMC1052 with a single-axis HMC1021Z. Both these magnetometers are made by Honeywell and provide a ± 6 gauss range. The differential output from these three axes were then passed to a unity gain operational amplifiers (OpAmps) in a differential configuration with the final analog voltage being fed to a Texas Instruments MSC1200Y2 microprocessor with an integrated 24 bit delta-sigma analog to digital converter ($\Delta\Sigma$ ADC). The three magnetometer readings were sampled at 100 samples per second (SPS) and the results recorded as the sensor set was rotated through various angles for a total of over 78,000 data points. Note that this resolution is far better than the sensor resolution from the data sheet, which would require only 19 bits, however, the ADC is low cost, and the extra bits are distributed as white noise. For more details on this hardware setup, see [8].

After recording data, the calibration algorithm discussed in this paper was used to generate calibration parameters and correct the raw data. The total Earth magnetic field at the point where this data was collected was found using [9]. Fig. 5 shows the raw data on the best fit calibration ellipsoid, and Fig. 6 shows the corrected results on a sphere with radius equal to the magnitude of the Earth's magnetic field. The calculated parameters for this sensor set are: $x_o = 262.73$, $y_o = -159.19$, $z_o = 23.01$, $a = 1.24\text{e}+8$,

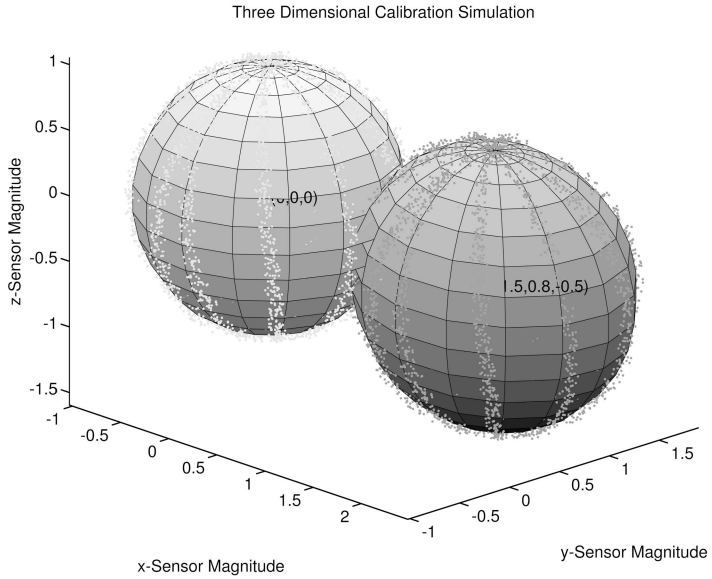

Fig. 4. Three-dimensional simulation of calibration procedure. Uncalibrated data on surface of rotated ellipsoid (lower right) and corrected data on surface of sphere with radius equal to field strength (upper left), both with center points labeled. Note that units here are in "Earth magnetic field equivalents," and that original offsets in simulation are $[1.5, 0.8, -0.5]$, which are recovered by the algorithm, along with scale factors and nonorthogonality. That is, a perfect sensor would show a sphere of radius 1.

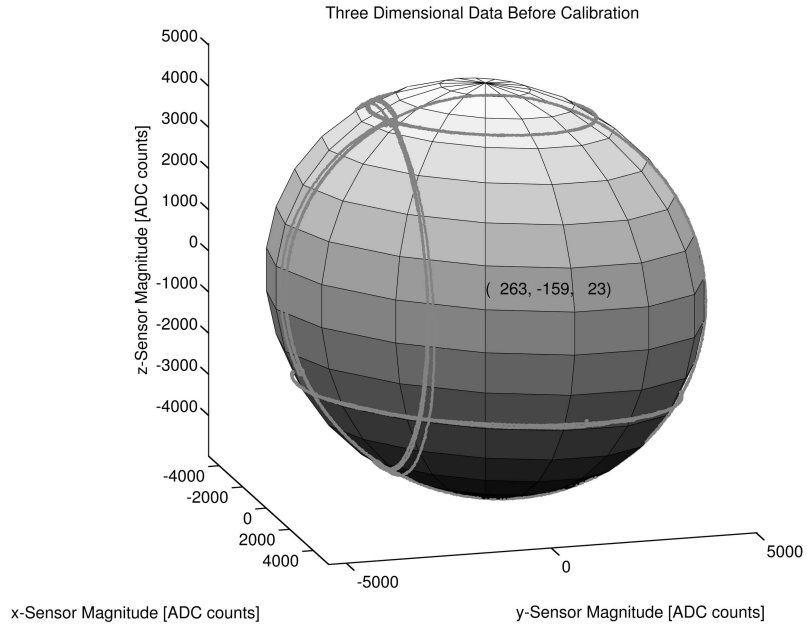

Fig. 5. Raw data from three-axis magnetometer plotted on estimation ellipsoid based on calibration parameters with center point labeled. Note that units here are in raw ADC counts, with center offset at $[263, -159, 23]$.

$b = 1.26\text{e}+8$, $c = 1.20\text{e}+8$, $\phi = -3.98°$, $\rho = 3.10°$, and $\lambda = -6.03°$.

Note here that the angular deviations for nonorthogonality are immediately recognizable in the size of their effect. The effect of the scale factor and null shift is harder to quantify in recognizable terms, however. In terms of heading angles, the results of this calibration result in a yaw angle deviation of approximately 0.25°. In terms of variation in the magnitude of the measured magnetic field, before calibration, the data shows a standard deviation of 0.0184 gauss; postcalibration, the same data shows a standard deviation of 0.00093 gauss, as shown in Fig. 7. This is an improvement by a factor of approximately 20!

VII. CONCLUSIONS

This paper has presented an expansion of the previously published nonlinear two-step calibration algorithm for solid-state strapdown magnetometers. We have expanded on the original error model, removed two assumptions on error sources, and solved for the calibration parameters using the

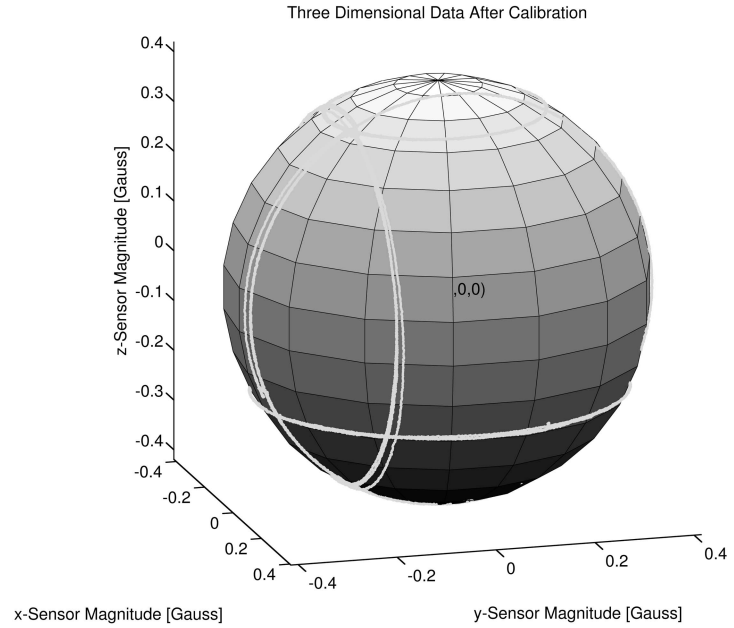

Fig. 6. Corrected data from three-axis magnetometer plotted on sphere with radius equal to Earth's magnetic field and center pointed labeled. Scale factors, biases, and nonorthogonality have all been removed from raw data. Note that units are now in gauss, as opposed to ADC counts in Fig. 5.

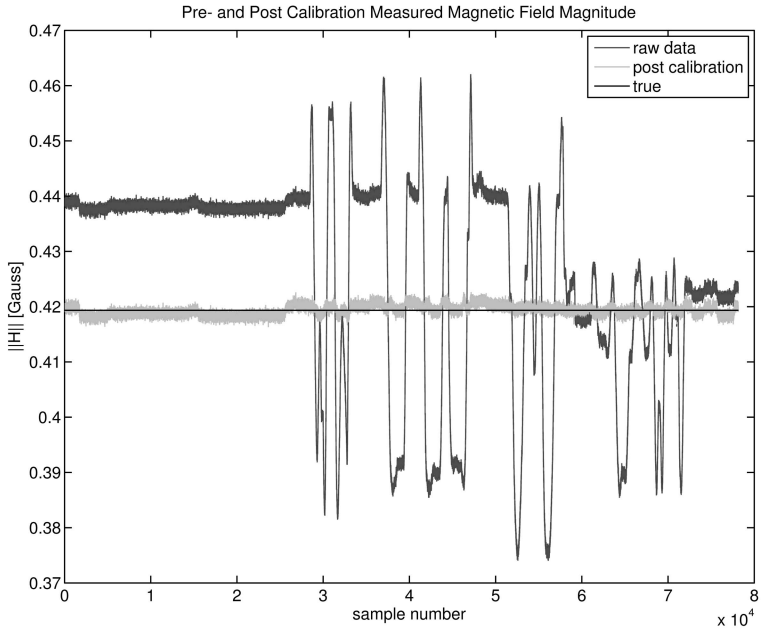

Fig. 7. Pre- and postcalibration magnitude of measured magnetic field. Note that before calibration, magnitude of magnetic field (which should be constant), varies with standard deviation of 1840.8 nT, and that postcalibration, this has been reduced to 93 nT.

same nonlinear two-step approach for both the two-dimensional and three-dimensional cases. The resulting algorithm now solves for angular misalignment parameters caused by both sensor misalignment and soft iron errors in the same body frame as the sensor set. Simulations and experimental data have been generated to show the success of the algorithm. In the case of the experimental data using a small low-cost three-axis magnetometer, the standard deviation of the magnetic field magnitude before calibration (1840.8 nT) improves by a factor of 20 once calibrated (93.1 nT).

Note that future work will include comparing this algorithm to the nonlinear expansion including all terms and optimized numerically using geometric numerical techniques. Also, we will install the sensor in a vehicle and use our technique as compared with conventional "swinging" to determine what improvement this technique yields when calibrating the full vehicle as opposed to just the sensor.

REFERENCES

[1] Caruso, M. J.
Aplication of magnetoresistive sensors in navigation systems.
SAE: Sensors and Actuators, (1997), 15–21.

[2] Gebre-Egziabher, D., Elkaim, G. H., Powell, J. D., and Parkinson, B. W.
A non-linear, two-step estimation algorithm for calibrating solid-state strapdown magnetometers.
Presented at the 8th International St. Petersburg Conference on Navigation Systems, St. Petersburg, Russia, 2001.

[3] Gebre-Egziabher, D., and Elkaim, G. H.
Calibration of strapdown magnetometers in magnetic field domain.
ASCE Journal of Aerospace Engineering, **19**, 2 (2006), 1–16.

[4] Bowditch, N.
The American Practical Navigator.
Defense Mapping Agnecy, Hydrographic/Topographic Center, Bethesda, MD, 1995.

[5] Gebre-Egziabher, D., and Elkaim, G. H.
MAV attitude determination from observations of Earth's magnetic and gravity field vectors.
AIAA Aerospace Electronic Systems Journal, submitted for publication.

[6] Gebre-Egziabher, D., Elkaim, G. H., Powell, J. D., and Parkinson, B. W.
A gyro-free, quaternion based attitude determination system suitable for implementation using low-cost sensors.
In *Proceedings of the IEEE Position Location and Navigation Symposium* (PLANS 2000), 185–192.

[7] G. M. K. Haupt, G. T., Kasdin, N. J., and Parkinson, B. W.
Optimal recursive iterative algorithm for discrete nonlinear least-squares problem.
AIAA Journal of Guidance Control and Navigation, (May–June 1996), 643–649.

[8] Foster, C. C., and Elkaim, G. H.
Development of the metasensor: A low-cost attitude heading reference system for use in autonomous vehicles.
Presented at the Institute of Navigation ION-GNSS Conference, Fort Worth, TX, 2006.

[9] Barton, C. E.
Revision of international geomagnetic reference field release.
EOS Transactions, (Apr. 1996).

Gabriel Hugh Elkaim received his B.S. degree in mechanical/aerospace engineering from Princeton University, Princeton, NJ, in 1990, the M.S. and Ph.D. degrees from Stanford University, Stanford, CA, in aeronautics and astronautics, in 1995 and 2002, respectively.

In 2003, he joined the faculty of the Jack Baskin School of Engineering, at the University of California, Santa Cruz, where he is an assistant professor in the Computer Engineering Department. His research interests include control systems, sensor fusion, GPS, system identification, and autonomous vehicle systems. His research focuses on intelligent autonomous vehicles, with an emphasis on robust guidance, navigation, and control strategies. Specifically, he has founded the Autonomous Systems Lab at UC Santa Cruz, and is currently developing an autonomous wing-sailed marine surface vehicle and off-road autonomous ground vehicles.

Christopher C. Foster received the Bachelor of Science degree in computer engineering with a minor in mathematics from Santa Clara University, Santa Clara, CA, in 2003 and the Masters of Science degree in computer engineering from the University of California, Santa Cruz in 2006, respectively.

He has been working in the defense industry since 2006. His research interests include high speed data collection, autonomous control, and embedded systems.